Proceedings of the 9th U.S. National and 10th Canadian Conference on Earthquake Engineering
Compte Rendu de la 9ième Conférence Nationale Américaine et
10ième Conférence Canadienne de Génie Parasismique
July 25-29, 2010, Toronto, Ontario, Canada • Paper No

SEISMIC BEHAVIOR AND MODELING OF FLAT-PLATE GRAVITY FRAMING IN TALL BUILDINGS

T.Y. Yang[1], G. Hurtado[2], and J.P. Moehle[3]

ABSTRACT

Concrete post-tensioned flat-plate framing is a prevalent "gravity framing" system in high-rise residential core-wall construction in North America. A common engineering practice has been to exclude this gravity framing from dynamic analysis models, but this practice is changing because of concerns about its participation. To study the effects, a laboratory test was conducted on a full-scale frame including the edge of a core wall, post-tensioned slab, and column. The test results demonstrated behavior of the framing and provided a basis for developing an analytical model for dynamic analysis of a tall core-wall building. The analytical model was subjected to bi-directional horizontal earthquake ground motions to study the effects of the slab-column-wall framing on building response as well as the effect of the building response on column axial loads.

Introduction

Cities on the West Coast of the United States experienced a surge in the construction of high-rise residential buildings at the start of the 21st century. Among these, concrete core walls with unbonded post-tensioned flat-plate framing became especially popular. The typical layout includes a centrally located core wall surrounded by perimeter columns (Figure 1a). This configuration enables flexible architectural layout, minimizes floor-to-floor height, and maximizes exterior views for building occupants. It also allows two concrete construction crews to work in parallel (Fig. 1b), with the first crew erecting the core wall several days ahead of a second crew constructing the flat plate and supporting columns. The parallel construction reduces total construction time and cost. It does, however, introduce a cold joint between the core wall and the surrounding flat plate.

Tall buildings using the core-wall/flat-plate framing combination typically exceed the height limit of the prescriptive provisions of the governing building code, and thus the design usually follows a performance-based approach. This performance approach generally requires demonstration, using nonlinear dynamic analysis, that the system will perform within safe limits under maximum considered earthquake (MCE) loading. The nonlinear dynamic analysis model usually includes only the core wall above grade, with the mass/weight of the above-grade gravity framing apportioned between the core wall and a P-delta column. (The core wall and below-grade diaphragms are modeled along with basement walls so the transfer of loads out of the core wall can be represented.) In this model it is assumed that the contribution of the slab-column-wall framing to structural resistance is negligible.

Three key questions arise. 1) What is the effect of the slab-column-wall framing on the dynamic

---

[1] Assistant Professor, Dept. of Civil Engineering, University of British Columbia, Vancouver, BC, Canada.
[2] Security Engineer, Applied Research Associates, Inc., Vicksburg, MS, USA.
[3] Professor, Dept. of Civil and Env. Engineering, University California, Berkeley, Berkeley, CA, USA.

response of the building? 2) Is the slab-column-wall framing, especially the cold joint between the slab and wall, sufficiently tough for imposed deformations? And 3) does the framing result in an accumulation of column axial loads (the so-called accidental outrigger effect) that might control the column design? The study reported in this paper was aimed at providing a perspective on each of these questions.
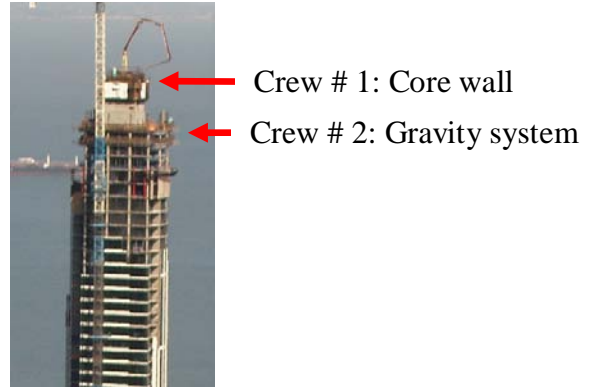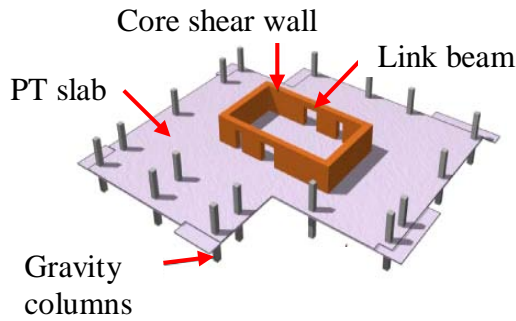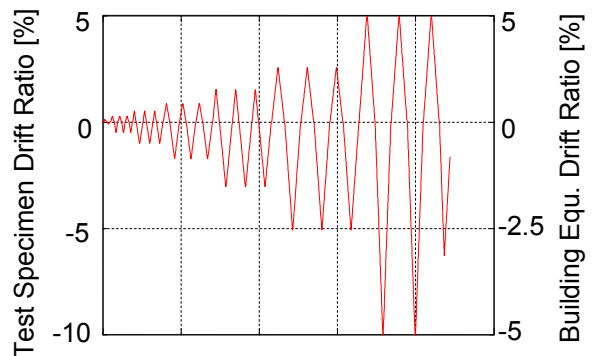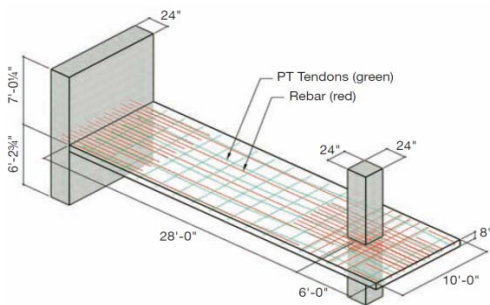

a) Typical isometric view of the floor plan (courtesy of MKA).

b) Typical construction scheme.

Figure 1. Typical concrete core wall with post-tensioned slab system.

Laboratory testing and analytical modeling of the gravity system

To study the seismic response of the slab-column-wall framing system, a laboratory test was conducted on a full-scale, 10-feet wide, internal frame including the edge of the concrete core wall, slab, and a perimeter column (Fig. 2a). The bases of the wall and column were pinned to the laboratory strong floor to permit rotations about an axis parallel to the base of the wall. Subsidiary gravity load (30.5 psf) in the form of lead weights was then distributed uniformly on the slab surface. A master actuator attached to the top of the wall imposed lateral displacements according to a target displacement history (Fig. 2b), while a slave actuator attached to the top of the column applied a lateral force equal to 70% of the force in the master actuator. Figure 3 shows an elevation view of the test setup.

a) Isotropic view of the test specemen.

b) Applied displacement loading history.

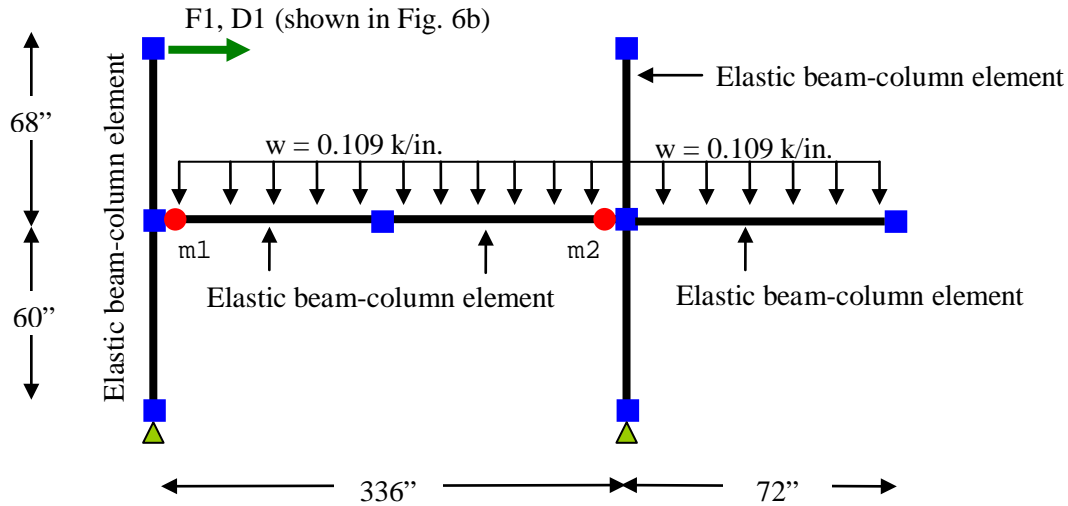Figure 2. Dimension of the specimen and displacement loading history.

Figure 3. Elevation view of the test setup (Klemencic et al. 2006).

The specimen was constructed using the typical construction sequence described previously. First, the full height of the core wall segment and the portion of the column beneath the slab were constructed. Lenton® Form Saver mechanical splices and intermittent shear keys were included as part of the wall construction. After a curing period for the wall and lower column, the slab and upper column were constructed. Finally, the post-tensioning tendons were stressed, and formwork and shores were removed. Figure 4 shows the slab-wall connection detail.

Figure 4. Slab-wall connection detail (Klemencic et al. 2006).

An analytical model of the test specimen (Fig. 5) was implemented using the lumped plastic-hinge model in the computer software Perform3D (CSI 2009). Slab, column, and wall spans were modeled with linearly elastic line elements, with nonlinear springs at slab ends. The nonlinear moment-curvature response of the hinge at the face of the wall (m_1) was calculated using a fiber section analysis with the expected material properties; because the post-tensioning tendons were anchored 8" from the face of the wall (Fig. 4), spring rotations were defined as the product of this 8" length and the calculated curvature. The nonlinear spring properties at the column end (m_2) were then calibrated using a trial and error procedure, in which the distributed gravity load (including the self weight and the added weight) was applied to the finite element model followed by a cyclic pushover analysis. Figure 6a shows the calibrated moment-rotation response of the plastic hinges. Figure 6b compares the measured and calculated force-deformation response of the test specimen. The result shows good match between the test data and analytical simulation.

Figure 5: Analytical model of the laboratory test specimen.

a) Plastic hinge properties.

b) Comparison of the force-deformation response of the test specimen.
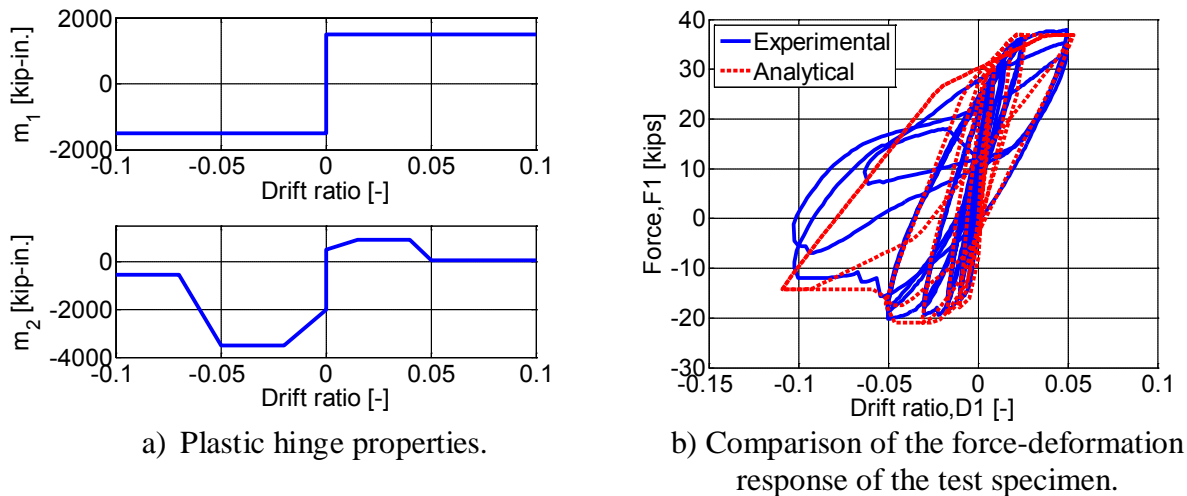
Figure 6: Force-deformation of the analytical model.

Description of the 48-story prototype model

A 48-story concrete core-wall building located in San Francisco, California was designed using a performance-based approach. The core wall was proportioned for design-level ground motions so that inelastic response would be restricted to flexural yielding of the wall at the base and the coupling beams over the height. An analytical model was developed using Perform3D. To reflect the design philosophy, nonlinear fiber wall section elements were used to model the lower quarter of the core wall while the remainder was modeled using linearly elastic fiber wall section elements. Coupling beams were modeled using the FEMA Beam, Concrete Type element in Perform3D (see Naish et al. 2009 for modeling details). Diaphragms at grade level and below were modeled using elastic shell elements. The basement walls were modeled as linear shear wall elements. Soil surrounding the basement was not modeled. Figure 7a shows the complete finite element model. Figure 7b shows the plan of a typical floor above grade.

a) Isotropic view of the finite element model.

b) Plan view of the finite element model. The broken boxes show individual columns included in the mega-columns.
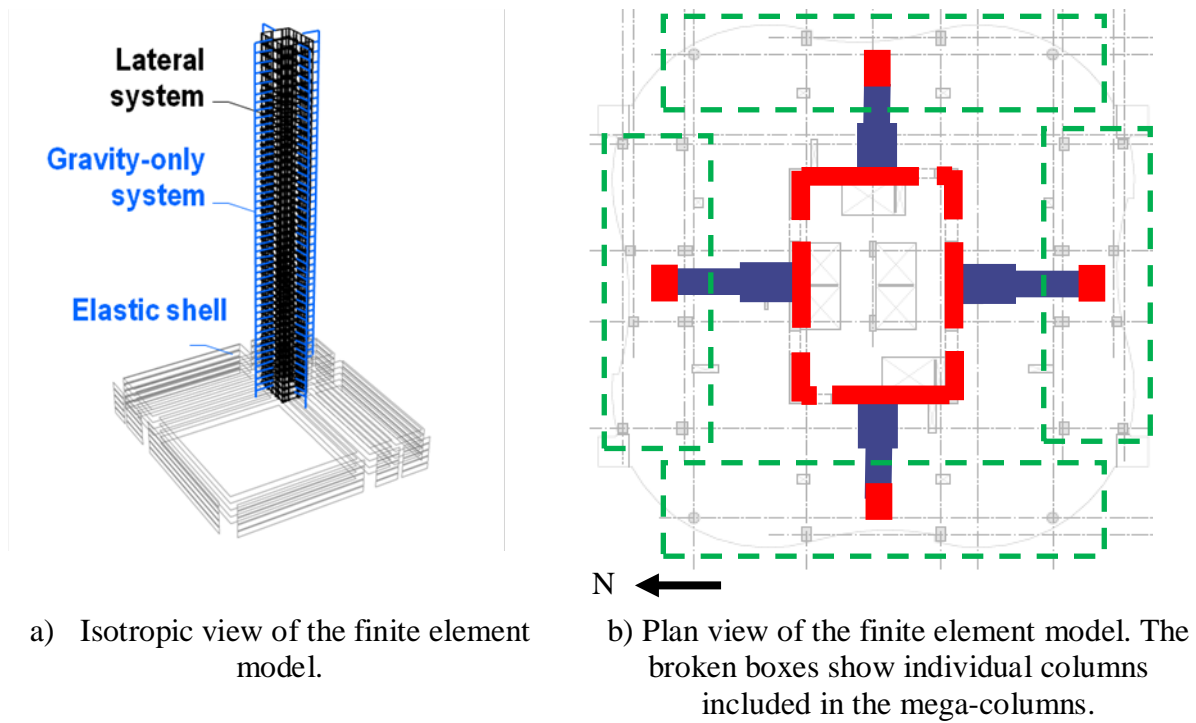
Figure 7: Isotopic and plan view prototype model.

To simplify the analytical model, the columns on each side of the building were modeled using linearly elastic mega-columns having axial and bending stiffnesses equal to the sums of stiffnesses of the adjacent individual columns. Flexural stiffness was reduced by a factor 0.5 to approximate cracking effects. The analytical model for the slabs was based on the calibrated lumped plastic hinge model (Fig 5). Because the analytical model was based on the test specimen, which was only 10 feet wide, several adjustments needed to be made:

1) The effective width of the slab at the slab-wall connection, b_{sw}, was estimated to be the wall length plus 10 feet on each side. The stiffness of the slab at the wall end was defined as the gross-section stiffness of this width. The nonlinear spring at the slab-wall connection had the same properties as spring m_1 of the analytical model of the test structure (Fig. 5) scaled by the factor $b_{sw}/10$ (the value 10 in the denominator is the width of the test model in feet).

2) The strength of the slab at the column side was taken as n times the strength of the spring m_2 used in the analytical model of the test structure, where n is the number of columns engaged by the slab at that side of the building. Here we assumed $n = 4$ in the north-south direction and 2 in the east-west direction.

3) The stiffness of the slab at the column end was calculated using the effective-beam-width model (Hwang and Moehle 2000). The effective width of an interior frame is thus.

$$b = n \times \max\left(2c_1 + \frac{l_1}{3}, l_2\right) \qquad (1)$$

in which max() = maximum function, c_1 = the depth of the column in the framing direction,

l_1 = distance between the inflection points in the framing direction (28 feet), and l_2 = distance between columns perpendicular to the framing direction (28 feet). Because the slab is post-tensioned, gross-section stiffness properties with this effective width were used.

4) Rather than applying the gravity load as distributed load on the gravity slab, the effect of the gravity load was modeled by apportioning tributary gravity loads as line elements on the walls and concentrated loads on the mega-columns, with any remaining load (associated with non-modeled gravity framing) applied to a centrally positioned P-delta column (an elastic column with high axial stiffness but low shear stiffness).

5) The strength of the slab at the slab-wall and slab-column connections was then adjusted to account for gravity moments. A linear-elastic finite element model of a typical bay was implemented using the software OpenSees (McKenna et al. 2000). Moments in the slab were calculated for expected gravity loads, then these moments were scaled up using the scaling procedures used in steps 1 and 2 above. The resulting moments were then subtracted from moment capacities of the nonlinear springs m_1 and m_2 (Fig. 6 a).

Selection and scaling of the ground motions

To study the seismic response of the prototype building, suites of ground motions were selected from the PEER NGA database (UCB 2009). The ground motions were selected to represent short-distance, large-magnitude earthquakes that are expected to have the largest impact to the design/performance of this structural system. The selected ground motions had the following characteristics: (1) Moment magnitude close to 7; (2) closest distance from fault between 0 and 20 km; (3) the longest usable period exceeding 8 sec; and (4) the spectrum shape similar to the target spectrum calculated using IBC2006 (ICC 2006) for the MCE hazard level in San Francisco. The selected ground motion pairs were amplitude scaled to approximately match the target spectrum in the period range 0.2T1 to 1.5T1. The first-mode period of the analytical model was T1 = 4.3 sec. Table 1 summarizes the ground motions selected for this study. Figure 8 shows the scaled SRSS response spectra and the associated scaling factors for each of the ground motion pairs.

Analytical simulation of the structural response

Expected gravity loads (1.0D + 0.25L) were first applied to the analytical model, followed by bi-directional shaking using the scaled ground motion pairs. The ground motions were not rotated but instead were applied to the model in the directions in which they were originally recorded. Rayleigh mass and stiffness proportional damping was set at 0.025 for periods equal to T1 and T1/10 (corresponding to approximately the third translational mode period).

Axial forces over the height of the mega-columns were calculated under several load cases, as shown in Fig. 9. All values are plotted negative (compression) because none of the columns was in tension for any load case. In addition to ground shaking simulations, a nonlinear static (pushover) analysis (with a load pattern proportional to the story height above the base) was carried out to lateral displacements sufficient to produce a full mechanism. The results from the ground shaking simulations are closely banded and lie close to the result from the nonlinear static analysis, suggesting that the slab-column-wall framing was yielding over nearly the full

height of the model at the times of maximum response.

Table 1.   Summary of the ground motions.

#	File Name	Earthquake	Station Name	Magnitude [Mw]	Vs30 [m/s]	Closest Dist. to Fault [km]
1	CapCPM	Cape Mendocino	Cape Mendocino	7.01	514	7.0
2	CapFOR	Cape Mendocino	Fortuna - Fortuna Blvd	7.01	457	20.0
3	CapPET	Cape Mendocino	Petrolia	7.01	713	8.2
4	DuzDZC	Duzce, Turkey	Duzce	7.14	276	6.6
5	GazGAZ	Gazli, USSR	Karakyr	6.80	660	5.5
6	KobAMA	Kobe, Japan	Amagasaki	6.90	256	11.3
7	KobFKS	Kobe, Japan	Fukushima	6.90	256	17.9
8	KobPRI	Kobe, Japan	Port Island	6.90	198	3.3
9	LomLGP	Loma Prieta	LGPC	6.93	478	3.9
10	LomSTG	Loma Prieta	Saratoga - Aloha Ave	6.93	371	8.5
11	LomWVC	Loma Prieta	Saratoga - W. Valley	6.93	371	9.3
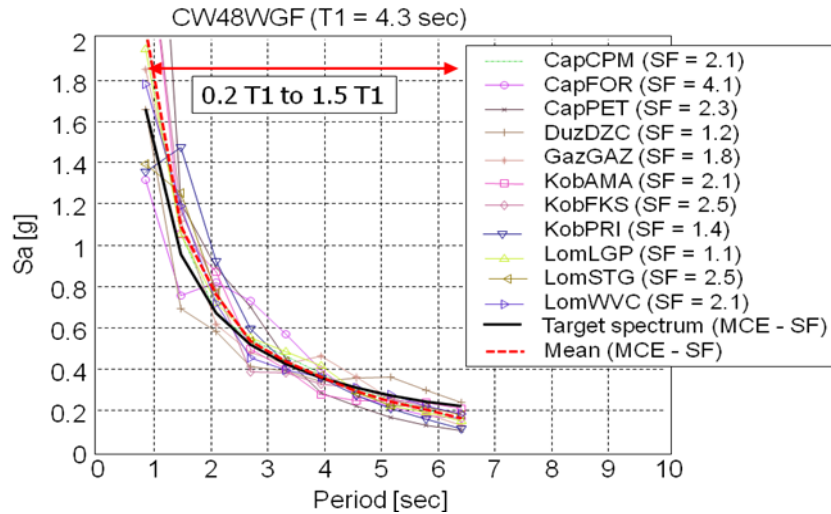
Figure 8: Selection and scaling of the ground motions. SF is the scaling factor.

The contribution of the earthquake to column axial loads was calculated by subtracting the contribution of the gravity load from the average maximum axial forces recorded from the ground shaking analyses. Figure 10a plots column axial forces due to dead (D), live (L), reduced live (Lred), and earthquake (E) effects. Figure 10b plots the design axial forces calculated using three commonly used design load combinations. The governing load case is 1.4D, followed by

the load case 1.2D + 1.6Lred, and then the load case 1.0D + 0.25L + 1.0 E. This result confirms that the gravity load combinations control the design of the columns for this case study building. Nevertheless, the axial load for the load combination including E is about 90% of the controlling load combination, suggesting that for other configurations (such as shorter post-tensioned slab span or higher slab moment capacity) the load combination including E might govern the column design. The results for the case study building suggest that simply summing the axial forces due to yielding over the full building height (as was done with the nonlinear static analysis) is a suitably quick way to check whether the seismic load combination is likely to control.
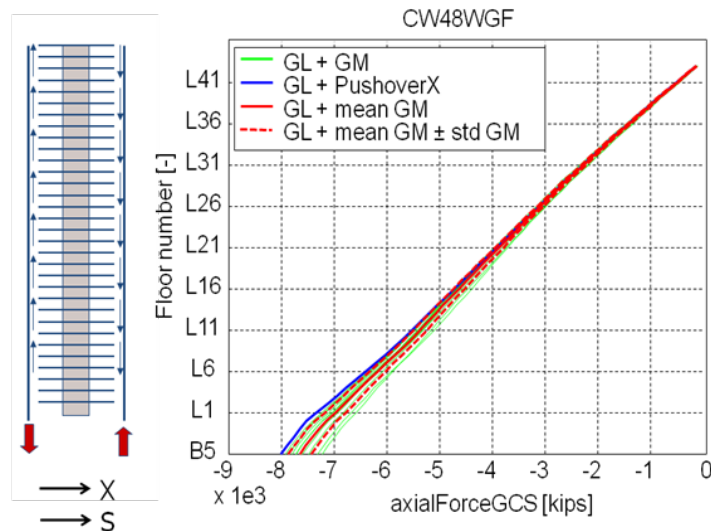
Figure 9: Maximum axial forces in the south side mega column. GL + GM is gravity load plus ground motion for individual earthquake simulations; GL + PushoverX is gravity load plus axial load under pushover analysis to large displacement; GL + mean GM is mean value of the individual GL + GM cases; GL + mean GM ± std GM is the mean plus or minus standard deviation value of the individual GL + GM cases.
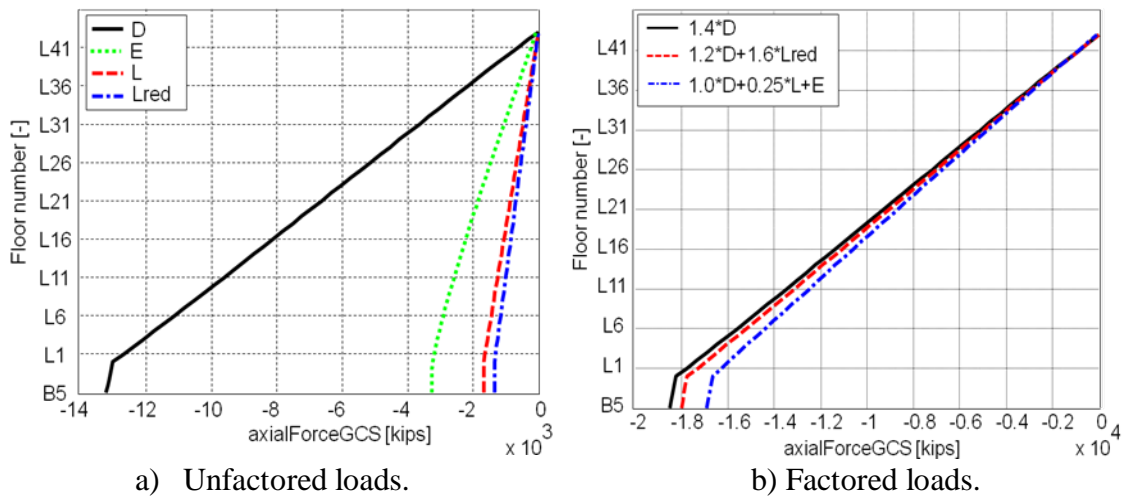

a) Unfactored loads.   b) Factored loads.

Figure 10: Axial forces in the south side mega column.

Effect on modeling the gravity systems

We also analyzed the seismic response of the core wall assuming the slab-column-wall gravity framing did not contribute to resistance, so that the effect of not including the gravity framing could be observed. Table 2 compares the periods for the first two translational modes (N-S and E-W direction) with and without the gravity framing included as part of the seismic-force-resisting system. Using the familiar approximation that period is proportional to the reciprocal of the square root of the stiffness, we can infer that the gravity framing resistance increases the stiffness by about 22% in the N-S direction and 13% in the E-W direction.

Table 2.   Comparison of the structural period and stiffness by including the gravity system.

	N-S direction	E-W direction
CW48NGF[+], T_i [sec]	4.72 sec	4.10 sec
CW48WGF*, T_i [sec]	4.27 sec	3.86 sec
% change in structural stiffness	22%	13%

[+] Without the gravity system. * With the gravity system.

The analytical model without the gravity framing resistance was again analyzed for the same ground motions and Rayleigh damping as were used previously (that is, no changes were made to accommodate the changes in periods). Figure 11 compares the mean of several peak responses with and without modeling the gravity system resistance. The effects on story drift, core wall shear, and core wall moment are negligible.
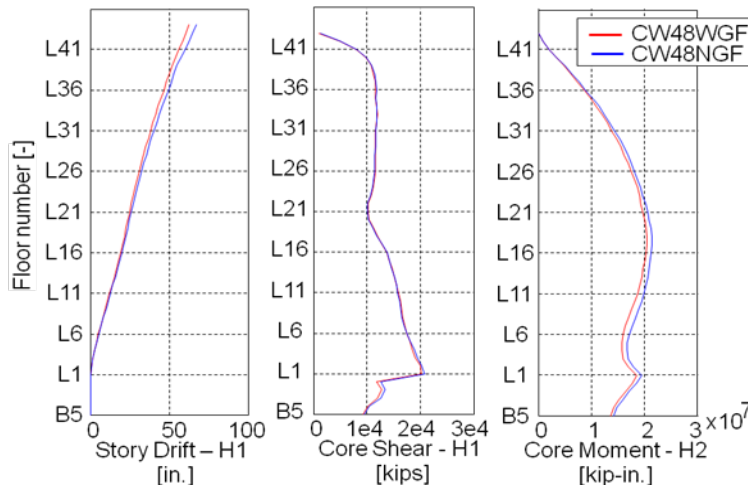

Figure 11: Comparison of the mean of the peak structural responses.

Summary and conclusions

A laboratory test on a full-scale slab-column-wall subassembly demonstrated that typical details of this framing system are capable of safely surviving deformations well beyond the design-level values for tall core-wall buildings. The results also provided a basis for calibrating an analytical model. The modeling approach was extended to develop an analytical model of a tall core-wall building. Within the limitations of the scope of this study, the results of nonlinear dynamic analysis suggest that: (a) accidental outriggering action of the gravity framing can result

in large column axial loads that may control the design of the columns, (b) the column axial load due to combined gravity and earthquake effects can be closely estimated by limit analysis assuming element hinging over the full height of the building, and (c) design of the core wall can be done ignoring the effects of slab-column-wall gravity framing resistance on the overall building response.

Acknowledgments

References

Klemencic, R., J.A. Fry, G. Hurtado, and J.P. Moehle, 2006. "Performance of post-tensioned slab-core wall connection," *PTI Journal*, Vol. 4, No. 2. Post-Tensioning Institute.

CSI, 2009. *Perform-3D*, Computers & Structures, Inc., Berkeley, CA.

Hwang, S.J., and J.P. Moehle, 2000. "Models for Laterally Loaded Slab-Column Frames," *ACI Structural Journal*, American Concrete Institute, title no. 97-S39.

ICC, 2006. *International Building Code*, International Code Council, Falls Church, Virginia.

McKenna, F., G.L. Fenves, M.H. Scott, and B. Jeremic, 2000. Open System for Earthquake Engineering Simulation (OpenSees), Pacific Earthquake Engineering Research Center, University of California, Berkeley.

UCB, 2009. NGA Database, Pacific Earthquake Engineering Research Center, University of California, Berkeley.

Naish, D., J.W. Wallace, J.A. Fry, R. Klemencic, 2009. "Reinforced concrete link beams: alternative details for improved construction", *SGEL Report*, 2009/06, University of California, Los Angeles.